Paleoceanography

Supporting Information for

Sea Surface Temperature reconstructions over the last 70 ky off Portugal: biomarker data and regional modeling

Sophie DARFEUIL[1], Guillemette MÉNOT[1], Xavier GIRAUD[1], Frauke ROSTEK[1], Kazuyo TACHIKAWA[1], Marta GARCIA[1], Édouard BARD[1]

[1]*Aix-Marseille Université, CNRS, IRD, Collège de France, CEREGE UM34; 13545 Aix-en-Provence, France*

Contents of this file

Additional Supporting Information (Files uploaded separately)

Introduction

This supporting information file contains supporting text (7 sections, Text S1-S7), 2 figures and 2 tables. Each section provides supporting information concerning 1. the new chronostratigraphy for core MD95-2042, 2. the age model justification, 3. the conversion of XRF-Calcium signal into %CaCO₃, 4. the new sampling of core MD95-2042 for this study, 5. the lipid extraction from marine sediment samples, 6. the alkenone analysis and the reliability of our new alkenone signals compared to those already published, 7. the evaluation of present and past simulations. The supporting figures provide further information relevant to the supporting texts S1 to S3, about the SpeleoAge model for core MD95-2042 (Figure S1), and the different signals on which this age model is based (Figure S2). The 2 tables contain the data used in the main text and in Figure S1. An additional table, too large for the supporting information, is the Dataset S1, given as an individual excel sheet and containing all the raw data for core MD95-2042 presented in the main text.

Text S1: New chronostratigraphy for core MD95-2042

Prior to any paleoclimatological study, a robust chronostratigraphy is required to establish a reference record. All previously published data for core MD95-2042 have been based on a wide diversity of age models founded on various methods [*Bard et al.*, 2004, 2013; *Cayre et al.*, 1999; *Daniau et al.*, 2007; *Eynaud et al.*, 2000, 2009; *Hinnov et al.*, 2002; *Hodell et al.*, 2010; *Moreno et al.*, 2002; *Pailler and Bard*, 2002; *Salgueiro et al.*, 2010; *Sánchez Goñi*, 2006; *Sánchez Goñi et al.*, 1999, 2000, 2002, 2005, 2008, 2009, 2013; *Shackleton et al.*, 2000, 2002, 2003, 2004; *Thouveny et al.*, 2000, 2004; *Voelker and de Abreu*, 2011]. The MD95-2042 age model can be improved and homogenized by providing a new, high-precision absolute time scale, made possible thanks to new available absolute dated chronologies, especially for older times outside the ^{14}C-dating period. Previous studies show a synchronous relationship between sedimentary $CaCO_3$ content and SST records from the Iberian Margin, Greenland $\delta^{18}O_{ice}$ record and Chinese speleothem $\delta^{18}O$ signals for the last 400 ky [*Barker et al.*, 2011; *Bard et al.*, 2013; *Hodell et al.*, 2013] (Text S2). Based on this relationship, we present a new chronostratigraphy from the present until mid-MIS 6 for core MD95-2042, by first converting its XRF-Calcium signal into $\%CaCO_3$ [*Pailler and Bard*, 2002], and then tuning it to the $\delta^{18}O$ of calcite of well-dated Chinese speleothems by U/Th method [*Wang et al.*, 2001, 2008; *Cheng et al.*, 2009].

To capture the rapid variability of $\%CaCO_3$ of core MD95-2042, Calcium XRF intensity was determined at 5mm resolution (corresponding to roughly 26 years) using an ITRAX core scanner (COX Analytical Systems) with a Mo tube at 30 kV and 45 mA, and with a 15s counting time. Analyses took place at CEREGE. The XRF intensity was then converted into $CaCO_3$ concentration using discrete measurements [*Pailler and Bard*, 2002] (Text S3).

The XRF-$\%CaCO_3$ millennial scale variability (Figure S2-C) was then tuned on continuous high-resolution U/Th absolute dated speleothem records from Chinese caves (Dongge Cave [*Dykoski et al.*, 2005], Hulu Cave [*Wang et al.*, 2001], Sanbao Cave [*Wang et al.*, 2008] and Linzhu Cave [*Cheng et al.*, 2009]), normalized by summer insolation at 65°N [*Berger and Loutre*, 1991] in order to highlight abrupt variability [*Barker et al.*, 2011] (Figure S2-B).

Twenty-four tie points between MD95-2042 XRF-$\%CaCO_3$ and insolation normalized speleothem $\delta^{18}O$ [*Barker et al.*, 2011] were chosen visually on the transitions of millennial-scale events (Table S1, Figure S2), and the match was performed with the AnalySeries 2.0.4.3 Linage software developed by *Paillard et al.* [1996]. The age model is piecewise linear between tie points (Figure S1). Existing ^{14}C data for core MD95-2042 [*Bard et al.*, 2013] are in agreement with our "SpeleoAge" tie points and piecewise linear age model (Figure S1).

All centennial- to millennial-scale events of the last glacial/interglacial cycle (Dansgaard/Oeschger Stadials/Interstadials and Heinrich Stadials) are observed in the XRF-$\%CaCO_3$ record (Figure S2-C), and are comparable to and in-phase with available Greenland isotopic signals on the GICC05 timescale for the last 60 ky [*Vinther et al.*, 2006; *Rasmussen et al.*, 2006; *Andersen et al.*, 2006; *Svensson et al.*, 2006, 2008] (Figure S2-A). Phasing discrepancies between MD95-2042 XRF-$\%CaCO_3$ and Greenland $\delta^{18}O_{ice}$ are larger (up to ~1 ky), going back farther in time (between 60 and 122 ka BP: GICC05modelext timescale for Greenland record [*Rasmussen et al.*, 2014; *Seierstad et al.*, 2014] (Figure S2-A)), due probably to greater age uncertainties for this ice age model. Independent, but still in agreement with Greenland records, this new age model for core MD95-2042 provides a robust absolute chronological framework for the Iberian Margin.

Text S2: Age model justification

In text S1, we present a new chronostratigraphy from the present to mid-MIS 6 for core MD95-2042, by tuning its XRF-Calcium signal converted into %CaCO$_3$ [*Pailler and Bard, 2002*] to the δ^{18}O of calcite of well-dated Chinese speleothems by U/Th method [*Wang et al., 2001, 2008; Cheng et al., 2009*].

It does not seem obvious that rapid variations of %CaCO$_3$ on the Iberian Margin are synchronous with Asian monsoon variations recorded by δ^{18}O of Chinese speleothems. Nevertheless, the missing link is Northern North Atlantic climate variations (recorded by Greenland δ^{18}O$_{ice}$), which play a pacemaker role, influencing both the mid-latitude North Atlantic Ocean and Asian monsoon position/intensity [*Zhang and Delworth, 2005*]. Recent studies based on δ^{18}O$_{ice}$, dust Ca^{2+}, δ^{15}N, CH$_4$ records measured in the same Greenland ice cores showed synchronous variations within half a century between Northern Atlantic temperatures and monsoon precipitations changes in Asia for abrupt climate variability of the last glacial and the last deglaciation [*Steffensen et al., 2008; Baumgartner et al., 2014*] (see *Bard et al.* [2013] for detailed explanations). Based on this hypothesis, a synthetic Greenland record was placed on the "SpeleoAge" timescale by correlating cold events in Greenland with weak monsoon events in the detrended speleothem record [*Barker et al., 2011*]. Furthermore, an unambiguous correlation has been demonstrated many times between planktic δ^{18}O and SST signals from the Iberian Margin cores and temperature variations in Greenland during the last glacial period [e.g. *Cayre et al., 1999; Shackleton et al., 2000; Pailler and Bard, 2002; Martrat et al., 2007; Barker et al., 2011*]. This led previous studies to tune the SST records from the Iberian Margin to Chinese speleothem δ^{18}O records [*Barker et al., 2011; Bard et al., 2013*]. Finally, variations in the XRF Ca/Ti signal for a core near to MD95-2042 were thought to be a reliable proxy for %CaCO$_3$ and were in phase with variations of planktic δ^{18}O and SST signals in the same core [*Hodell et al., 2013*], as already detected by *Pailler and Bard* [2002] on the Iberian Margin area. Therefore, we are able to tie Iberian Margin sediment records such as %CaCO$_3$ to absolute dated speleothem records in order to place core MD95-2042 signals on a SpeleoAge timescale.

Text S3: Conversion of XRF-Ca intensity into quantitative % CaCO$_3$

The raw XRF Ca-signal was smoothed by the least squares 2-3 procedure on 11 points [*Savitzky and Golay, 1964*] to keep inflexion points at their original position. We used discrete measurements of %CaCO$_3$ on core MD95-2042 from *Pailler and Bard* [2002], to calibrate and convert the smoothed XRF calcium signal into %CaCO$_3$. The high degree of linear correlation (n=310, R^2=0.90) between % of calcium and % of carbonates justifies the assumption that most Ca^{2+} and CO$_3^{2-}$ are associated in the form of CaCO$_3$.

Iberian Margin giant sediment cores extracted with the Calypso piston coring system onboard R/V *Marion Dufresne* are known to be stretched in the upper part (from the top until 5 to 15 meters depth), which has an effect on the magnetic fabric sediment data [*Hall and McCave, 2000; Thouveny et al., 2000; Moreno et al., 2002; Skinner and McCave, 2003*]. This piston suction and consecutive sediment extension in core MD95-2042 is particularly substantial until 10 meters depth downcore, as observed by the K max inclination parameter [*Thouveny et al., 2000*]. This sediment stretching may impact the XRF semi-quantitative measurements of Ca, and bias our %CaCO$_3$ reconstructions. Thus, in order to convert MD95-2042 Ca-signal into high resolution carbonate contents (%CaCO$_3$), we compared the efficiency of a single linear equation for the whole core (n=310, R^2=0.90) to two linear calibration equations: one for [0 m – 10 m] (influenced by piston suction) (n=97, R^2= 0.87) and one for [10 m - 31.4 m] (non stretched sediment) (n=213, R^2=0.94).

The sum of the %CaCO$_3$ squared residues on the total length of core MD95-2042 is significantly smaller while using two linear calibrations instead of one (Fisher test on the residues: n=310, p<0.018). Therefore, we used the two linear equations to reconstruct high-resolution XRF-derived %CaCO$_3$ for core MD95-2042 (Figure 2-C).

Text S4: New sampling of core MD95-2042 for biomarker analysis

Core MD95-2042 was sampled initially in 1996 and the entire core was sliced at 1 cm spacing; the resulting samples have been stored at 4°C since then in plastic bags. An alkenone record for core MD95-2042 was previously measured by GC in 1998 and published by *Pailler and Bard* [2002]. For this new paper, we duplicated the original U^K_{37} record and doubled its resolution every 5 cm, equivalent to an average time resolution of 260 years. The new sampling of the core was performed in 2012 on the 1 cm subsamples stored in plastic bags. A total of 401 sediment samples were thus aliquoted over the upper 19.60 meters of the core, corresponding to the last 70 ka. The samples were then freeze-dried under vacuum and finely ground in an agate mortar before molecular extraction and analysis.

Text S5: Lipid extraction

For biomarker analyses, 2 g of dried homogenized ground sediment were extracted with the accelerated solvent extraction method (ASE 200, Dionex) using dichloromethane/methanol (90:10 v/v) at 120°C and 80 bars, following the procedure described in *Pailler and Bard* [2002]. Before extraction, known amounts of ethyl-triacontanoate (C32) and C46-GDGT were added as internal standards. A known amount of n-hexatriacontane (C36) was added to the obtained total lipid extracts (TLE), as an external standard to quantify the extraction yield for alkenones (average of 95% and standard deviation of 19%; n=400). Thereafter, the TLE were subdivided into two identical aliquots, for alkenone analysis, and for subsequent purification before GDGT analysis.

Text S6: Alkenone analyses and reliability of our new record

Gas chromatography analysis of alkenones was performed by means of a *Thermo Scientific Trace GC* equipped with a flame ionization detector (FID). Analytical conditions are similar to those described by *Sonzogni et al.* [1997]. The purity of $C_{37:2}$ and $C_{37:3}$ alkenones was checked on selected samples by GC-MS using a Trace GC coupled to a DSQII quadrupole mass spectrometer (*Thermo Electron*) with similar GC conditions but using helium as the carrier gas. Quantification of di- and tri-unsaturated C_{37} alkenones was made by peak integration of GC chromatograms and by assuming the same response factor for analytes as for the internal standard C32. Concentrations of di and tri-unsaturated C_{37} alkenones are given as sum in µg/g of dry weight sediment. The U^k_{37} was calculated according *Prahl and Wakeham* [1987].

The precision of our analytical procedures for the SST determination had been assessed in the frame of the international alkenone intercomparison [*Rosell-Melé et al.*, 2001]. A large sediment sample from the core catcher of MD95-2042 was homogenized in order to further check the precision and accuracy of biomarker analyses. Aliquots were measured over the period 2012 to 2014, exceeding the dataset acquisition of the present paper. The 40 replicates resulted in a mean U^K_{37} of 0.557 (equivalent to 15.25 °C) with a standard deviation of 0.010 (0.26 °C) (n = 40), and an

alkenone concentration of 184 ng/g sed. with a standard deviation of 27 ng/g sed. (n = 39), agreeing with previous measurements in 1998 (mean $U^{K'}_{37}$: 0.541 (14.76 °C) with a standard deviation of 0.015 (0.45 °C); alkenone concentration: 276 ng/g sed. with a standard deviation of 42 ng/g sed; n=3).

The new high-resolution alkenone record agrees with the one measured in 1998 [Pailler et Bard, 2002] as illustrated by the mean differences between the two datasets ($\Delta U^{K'}_{37}$ = -0.012 (-0.34 °C); ΔC_{37}tot = -69 ng/g sed. (i.e. -10 % of the mean value), n= 193). These mean differences are smaller than the analytical errors usually reported for alkenone measurements in fully marine environments (e.g. standard deviations for $U^{K'}_{37}$ = 0.017 (0.5°C), and for C_{37}tot = 28% for ocean sediment standard samples A, B and D in Rosell-Melé et al. [2001]), but with a larger dispersion than expected with $\Delta U^{K'}_{37}$ standard deviations of 0.039 (1.1 °C) and 49 % of the mean value of both C_{37}tot measurements.

The lack of systematic shifts in the two datasets for both standard sediment and downcore samples, rules out a significant laboratory degradation of alkenones in core MD95-2042 over the last 15 years. This is a precautionary step because laboratory degradation of alkenones and disturbance of $U^{k'}_{37}$ index have been noted and experimentally tested in our lab for marine sediment samples conserved at high temperature (50°C) or under UV light for prolonged time periods (data not shown). Nevertheless, the largest differences are associated with the lowest concentrations, notably during H1, H2 and H3 events (Figure 3-B and D). This rather points to an analytical difference, since low-concentration samples (<0.3µg/g sed.) are more difficult to quantify accurately [Rosell-Melé et al., 2001].

Therefore, the lack of a consistent shift between the datasets measured in 1998 and 2013 justifies that this paper is based upon the new high-resolution alkenone record.

Text S7: Evaluation of present and paleo simulations

The validity of simulated ocean physics, especially in terms of temperature and currents, is a crucial point which needs to be assessed prior to any consideration of Tproxy results. Indeed, Tproxies record modeled in situ temperature when their mass is produced, and they undergo advection through surface and subsurface currents prior to export to the seafloor.

Our modeled Present Day (PD) circulation reproduces the Azores Current (AzC), the Portugal Current (PC) and the starting point of the Canary Current (CC) (Figure 1-B1), as well as coastal transition zone seasonality (winter poleward flow and summer upwelling-associated, equatorward flow). This is coherent both with observations and also with a previous study showing that whatever the modern forcing for ROMS on the Iberian Basin (9 GCMs and COADS climatology tested), these seasonal circulation features are always represented for present day simulations [Pires et al., 2014]. The resolution of ROMS (1/10°) reproduces fine seasonal oceanic structures specific to the Iberian Margin that cannot be captured by the coarser resolution of global climatologies (e.g. COADS resolution = 0.5°x0.5°, World Ocean Atlas 2005 resolution = 1°x1°) or General Circulation Models (e.g. IPSL-CM4 resolution = 2°x1.5°, Figure 1-C). This high resolution (1/10° ≈ 9km) of the regional model allows direct comparison in terms of temperature with satellite SST climatologies. The modeled PD annual mean SSTs (Figure 1-B1) are comparable (±1°C) to the 9km-resolution satellite SST (Pathfinder climatology [Casey and Cornillon, 1999; Armstrong and Vazquez-Cuervo, 2001]), except along the coast (-2.5°C) due to an overestimation of the summer upwelling (coast-to-offshore gradient increase of 5°C in August). Similarly, PD annual mean subsurface temperatures (mean from surface to 200m depth) are analogous (±1°C) to those recorded in the World Ocean Atlas 2005 [Locarnini et al., 2006], but are slightly colder (-2.5°C) along

the coast, due to the summer upwelling. At the site of the core (offshore the upwelling zone), comparable (maximum ±1.5°C) temperature variations and seasonal amplitudes are observed for both the model and climatologies (~6°C for SST and ~1.5°C for the 0-200m interval), for annual or monthly means, as well as for surface or subsurface depth interval (Figure 7-A1 and Table 2).

LGM and HS surface and subsurface circulations also exhibit strong seasonality, with the maintenance of the summer upwelling and winter poleward circulation along the coast, but without the sizeable offshore currents (PC, AzC, CC) (Figure 1-B2 and B3). In the same way as for PD, the annual mean SSTs from ROMS paleo simulations are about 1°C lower than the associated IPSL-CM4 simulations, and about 1.5°C colder along the coast due to summer upwelling occurrence in the regional simulations in contrast to the GCM. ROMS annual mean 0-200m paleo temperatures give comparable results (±0.5°C) to their IPSL-CM4 forcings, but are slightly colder (up to -1°C) along the coast during summer coastal upwelling. Again, MD95-2042 core site is offshore the transition zone, and surface and subsurface temperatures do not exhibit differences with IPSL-CM4 larger than 1.5°C and 0.5°C respectively, with comparable seasonality (Figure 7-A2 and A3 and Figure 5). In the North Atlantic Ocean and Europe, at Iberian latitudes, IPSL-CM4 in the LGM mode gives temperature results comparable to various paleoclimatic records for the corresponding climate state (MARGO database for SST, and pollen data for continental temperatures) [Kageyama et al., 2006]. Moreover, other studies comparing IPSL-CM4 results (in LGM and/or HS mode) with associated proxy data show reasonable agreement [Otto-Bliesner et al., 2009; Mariotti et al., 2012; Kageyama et al., 2009, 2013a, 2013b; Mariotti, 2013; Marzin et al., 2013; Woillez et al., 2013], further validating IPSL-CM4 outputs for LGM and HS modes. Therefore, as IPSL-CM4 is thought to represent past climatology and hydrology reasonably well, and ROMS outputs give comparable results to this GCM, we consider that ROMS paleo simulations give a reasonable paleohydrology for LGM and HS upon which Tproxy signals are based.
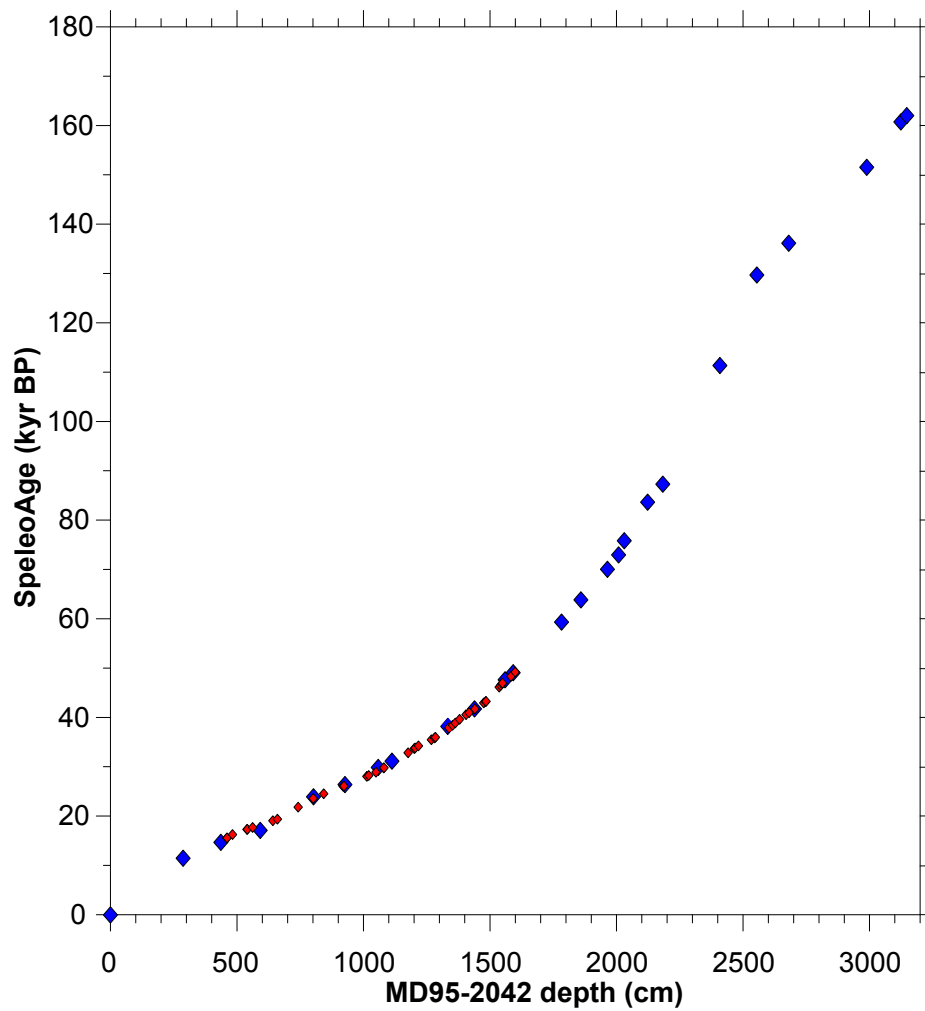
Figure S1. *New SpeleoAge model for core MD95-2042: piecewise linear between tie points (blue diamonds). Small red diamonds are MD95-2042 ^{14}C cal. ages* **[Bard et al., 2013]**.
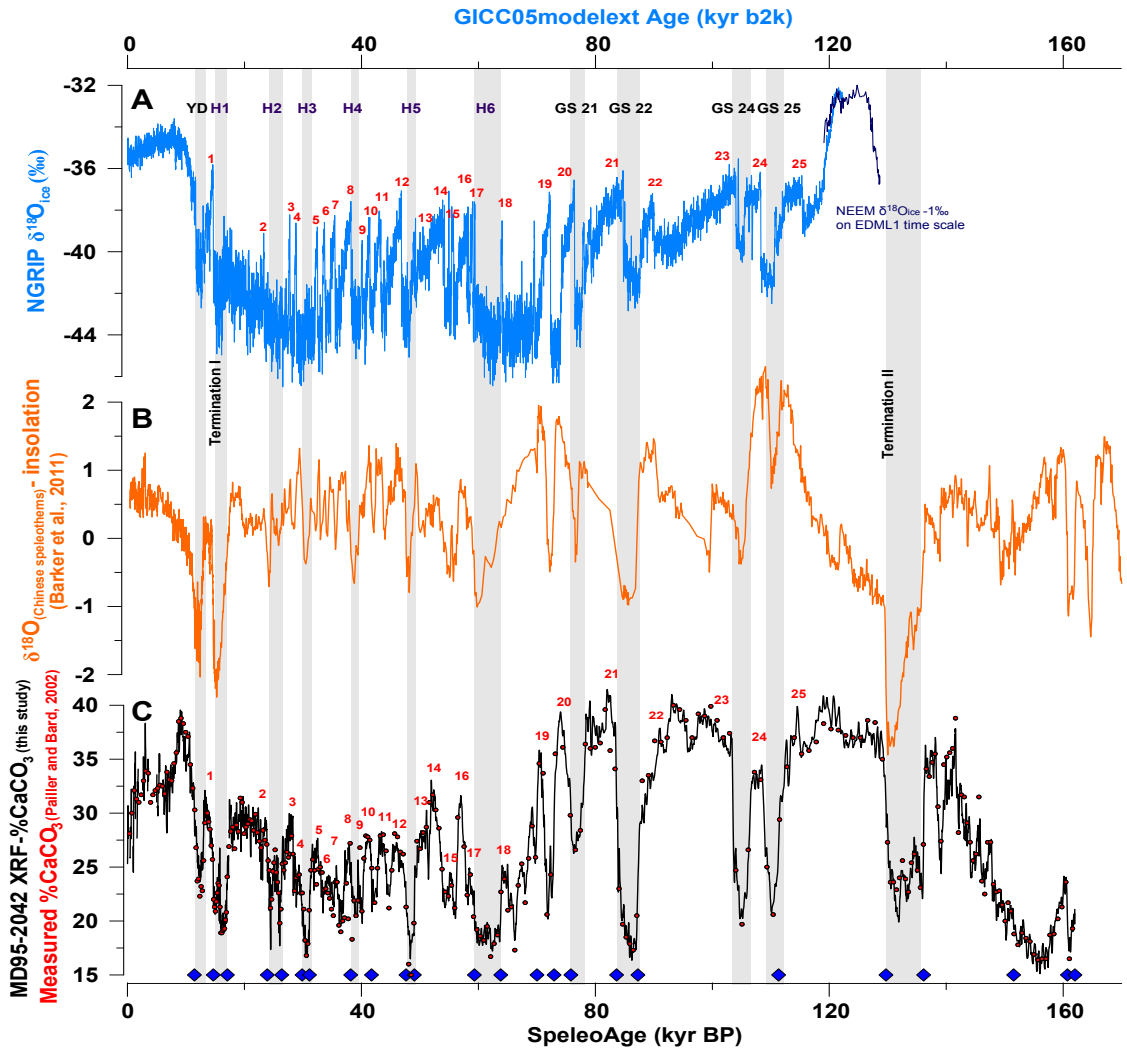
Figure S2. Tuning assessment for core MD95-2042. (A) NGRIP $\delta^{18}O_{ice}$ (blue) on the GICC05modelext timescale (GICC05: [Vinther et al., 2006] for 0 – 7.9 kyr b2k, [Rasmussen et al., 2006] for 7.9 – 14.7 kyr b2k, [Andersen et al., 2006; Svensson et al., 2006] for 14.7 – 41.8 kyr b2k, [Svensson et al., 2008] for 41.8 – 60 kyr b2k; GICC05modelext: [Rasmussen et al., 2014; Seierstad et al., 2014] for 60 – 122 kyr b2k), NEEM $\delta^{18}O_{ice}$ – 1‰ (dark blue) on EDML1 time scale for 114 – 128 kyr b2k [NEEM Community Members, 2013]; (B) Absolute dated Chinese speleothem $\delta^{18}O$ normalized by insolation at 65°N in June (orange) on the SpeleoAge timescale [Barker et al., 2011]; (C) MD95-2042 XRF-%CaCO₃ (black) (this study) and measured %CaCO₃ (red dots) [Pailler and Bard, 2002] on the SpeleoAge timescale. Blue diamonds are the tie points chosen by visual matching on Analyseries [Paillard et al., 1996] between MD95-2042 XRF-%CaCO₃ signal and the insolation normalized Chinese speleothem $\delta^{18}O$ [Barker et al., 2011]. Grey bars refer to cold events: YD= Younger Dryas, H1 = Heinrich Stadial 1. Red numbers refer to warm Dansgaard/Oeschger events also called Greenland InterStadial (GIS) events.

Climatic event corresponding to tie-point position (named after Martrat et al., 2007 Science)	Marine Isotopic Stage (MIS)	MD95-2042 tie points (depth, cm)	SpeleoAge (ka BP)
Core top	MIS 1	0.0	-0.045
End YD	MIS 1	287.2	11.451
Start BA/End H1 (Termination I)	MIS 1/MIS 2	436.3	14.677
Start H1	MIS 2	592.0	17.354
End H2	MIS 2	802.6	23.907
Start H2 (End DO3')	MIS 2/MIS3	926.9	26.385
End H3 (Start DO4)	MIS 3	1058.2	29.859
Start H3 (End DO5')	MIS 3	1112.7	31.132
End H4 (Start DO8)	MIS 3	1333.1	38.174
Start DO10	MIS 3	1438.9	41.732
End H5 (Start DO12)	MIS 3	1559.7	47.628
Start H5	MIS 3	1591.8	49.060
End H6 (Start DO17)	MIS 4	1782.9	59.326
Start H6 (End DO18)	MIS 4	1859.4	63.833
End DO19	MIS 5a	1964.3	70.028
End DO20	MIS 5a	2008.4	72.950
Start DO20	MIS 5a	2030.8	75.821
Start DO21	MIS 5a/MIS 5b	2123.1	83.636
End DO22	MIS 5b/MIS 5c	2183.1	87.287
End DO25	MIS 5d/MIS 5e	2408.8	111.341
Termination II	MIS 5e/MIS 6	2554.8	129.693
End DO1	MIS 6	2680.8	136.136
Start DO2	MIS 6	2989.1	151.528
Start DO3	MIS 6	3124.0	160.724
End DO4	MIS 6	3147.4	162.001

Table S1. *Position of each tie point for MD95-2042 chronology, its associated SpeleoAge (kyr BP) and climatic event. H= Heinrich Stadial, DO= Dansgaard/Oeschger interstadial*

Climate mode	ROMS physics			Tproxy					
	Forcings	Simulation time	Simulation time	Annual	Summer	Winter	Annual	Summer	Winter
				Surface Production			0-200m Production		
PD	WOA 2005 COADS	125 years	y111-y125	PD_ASP	PD_SSP	PD_WSP	PD_ADP	PD_SDP	PD_WDP
LGM	'LGM' IPSL-CM4	125 years	y111-y125	LGM_ASP	LGM_SSP	LGM_WSP	LGM_ADP	LGM_SDP	LGM_WDP
HS	'FWF' IPSL-CM4	125 years	y111-y125	HS_ASP	HS_SSP	HS_WSP	HS_ADP	HS_SDP	HS_WDP

Table S2. *Conducted ROMS simulations and Tproxy experimentation*

Data Set S1. MD95-2042 data: XRF and biomarkers results

References:

Andersen, K. K. et al. (2006), The Greenland Ice Core Chronology 2005, 15–42 ka. Part 1: constructing the time scale, *Quat. Sci. Rev.*, *25*(23–24), 3246–3257, doi:10.1016/j.quascirev.2006.08.002.

Armstrong, E. M., and J. Vazquez-Cuervo (2001), A new global satellite-based sea surface temperature climatology, *Geophys. Res. Lett.*, *28*(22), 4199–4202, doi:10.1029/2001GL013316.

Bard, E., F. Rostek, and G. Ménot-Combes (2004), Radiocarbon calibration beyond 20,000 14C yr B.P. by means of planktonic foraminifera of the Iberian Margin, *Quat. Res.*, *61*(2), 204–214, doi:10.1016/j.yqres.2003.11.006.

Bard, E., G. Menot, F. Rostek, L. Licari, P. Boening, R. L. Edwards, H. Cheng, Y. Wang, and T. J. Heaton (2013), Radiocarbon Calibration/Comparison Records Based on Marine Sediments from the Pakistan and Iberian Margins, *Radiocarbon*, *55*(4), 1999–2019, doi:10.2458/azu_js_rc.55.17114.

Barker, S., G. Knorr, R. L. Edwards, F. Parrenin, A. E. Putnam, L. C. Skinner, E. Wolff, and M. Ziegler (2011), 800,000 Years of Abrupt Climate Variability, *Science*, *334*, 347–351, doi:10.1126/science.1203580.

Baumgartner, M. et al. (2014), NGRIP CH4 concentration from 120 to 10 kyr before present and its relation to a δ15N temperature reconstruction from the same ice core, *Clim Past*, *10*(2), 903–920, doi:10.5194/cp-10-903-2014.

Berger, A., and M. Loutre (1991), Insolation Values for the Climate of the Last 10000000 Years, *Quat. Sci. Rev.*, *10*(4), 297–317, doi:10.1016/0277-3791(91)90033-Q.

Casey, K. S., and P. Cornillon (1999), A comparison of satellite and in situ-based sea surface temperature climatologies, *J. Clim.*, *12*(6), 1848–1863, doi:10.1175/1520-0442(1999)012<1848:ACOSAI>2.0.CO;2.

Cayre, O., Y. Lancelot, and E. Vincent (1999), Paleoceanographic reconstructions from planktonic foraminifera off the Iberian Margin: Temperature, salinity, and Heinrich events, *Paleoceanography*, *14*(3), 384–396, doi:10.1029/1998PA900027.

Cheng, H., R. L. Edwards, W. S. Broecker, G. H. Denton, X. Kong, Y. Wang, R. Zhang, and X. Wang (2009), Ice Age Terminations, *Science*, *326*(5950), 248–252, doi:10.1126/science.1177840.

Daniau, A., M. Sanchez-Goni, L. Beaufort, F. Laggoun-Defarge, M. Loutre, and J. Duprat (2007), Dansgaard-Oeschger climatic variability revealed by fire emissions in southwestern Iberia, *Quat. Sci. Rev.*, *26*(9-10), 1369–1383, doi:10.1016/j.quascirev.2007.02.005.

Dykoski, C. A., R. L. Edwards, H. Cheng, D. Yuan, Y. Cai, M. Zhang, Y. Lin, J. Qing, Z. An, and J. Revenaugh (2005), A high-resolution, absolute-dated Holocene and deglacial Asian

monsoon record from Dongge Cave, China, *Earth Planet. Sci. Lett.*, *233*(1–2), 71–86, doi:10.1016/j.epsl.2005.01.036.

Eynaud, F., J. L. Turon, M. F. Sánchez-Goñi, and S. Gendreau (2000), Dinoflagellate cyst evidence of "Heinrich-like events" off Portugal during the Marine Isotopic Stage 5, *Mar. Micropaleontol.*, *40*(1-2), 9–21, doi:10.1016/S0377-8398(99)00045-6.

Eynaud, F. et al. (2009), Position of the Polar Front along the western Iberian margin during key cold episodes of the last 45 ka, *Geochem. Geophys. Geosystems*, *10*(7), doi:10.1029/2009GC002398.

Hall, I. R., and I. N. McCave (2000), Palaeocurrent reconstruction, sediment and thorium focussing on the Iberian margin over the last 140 ka, *Earth Planet. Sci. Lett.*, *178*(1–2), 151–164, doi:10.1016/S0012-821X(00)00068-6.

Hinnov, L. A., M. Schulz, and P. Yiou (2002), Interhemispheric space–time attributes of the Dansgaard–Oeschger oscillations between 100 and 0 ka, *Quat. Sci. Rev.*, *21*(10), 1213–1228, doi:10.1016/S0277-3791(01)00140-8.

Hodell, D., S. Crowhurst, L. Skinner, P. C. Tzedakis, V. Margari, J. E. T. Channell, G. Kamenov, S. Maclachlan, and G. Rothwell (2013), Response of Iberian Margin sediments to orbital and suborbital forcing over the past 420 ka, *Paleoceanography*, n/a–n/a, doi:10.1002/palo.20017.

Hodell, D. A., H. F. Evans, J. E. T. Channell, and J. H. Curtis (2010), Phase relationships of North Atlantic ice-rafted debris and surface-deep climate proxies during the last glacial period, *Quat. Sci. Rev.*, *29*(27–28), 3875–3886, doi:10.1016/j.quascirev.2010.09.006.

Kageyama, M. et al. (2006), Last Glacial Maximum temperatures over the North Atlantic, Europe and western Siberia: a comparison between PMIP models, MARGO sea–surface temperatures and pollen-based reconstructions, *Quat. Sci. Rev.*, *25*(17–18), 2082–2102, doi:10.1016/j.quascirev.2006.02.010.

Kageyama, M., J. Mignot, D. Swingedouw, C. Marzin, R. Alkama, and O. Marti (2009), Glacial climate sensitivity to different states of the Atlantic Meridional Overturning Circulation: results from the IPSL model, *Clim. Past*, *5*(3), 551–570, doi:10.5194/cp-5-551-2009.

Kageyama, M. et al. (2013a), Mid-Holocene and Last Glacial Maximum climate simulations with the IPSL model—part I: comparing IPSL_CM5A to IPSL_CM4, *Clim. Dyn.*, *40*(9-10), 2447–2468, doi:10.1007/s00382-012-1488-8.

Kageyama, M. et al. (2013b), Mid-Holocene and last glacial maximum climate simulations with the IPSL model: part II: model-data comparisons, *Clim. Dyn.*, *40*(9-10), 2469–2495, doi:10.1007/s00382-012-1499-5.

Locarnini, R. A., A. V. Mishonov, J. I. Antonov, T. P. Boyer, and H. E. Garcia (2006), *World Ocean Atlas 2005, Volume 1: Temperature*, Ed. NOAA ATlas NESDIS 61., S. Levitus, U.S. Gov. Printing Office, Washington, D.C.

Mariotti, V. (2013), Modélisation du cycle du carbone en climat glaciaire: état moyen et variabilité, Thèse de Doctorat, Université de Versailles Saint-Quentin, LSCE, Gif-sur-Yvette.

Mariotti, V., L. Bopp, A. Tagliabue, M. Kageyama, and D. Swingedouw (2012), Marine productivity response to Heinrich events: a model-data comparison, Clim Past, 8(5), 1581–1598, doi:10.5194/cp-8-1581-2012.

Martrat, B., J. Grimalt, N. Shackleton, L. de Abreu, M. Hutterli, and T. Stocker (2007), Four climate cycles of recurring deep and surface water destabilizations on the Iberian margin, Science, 317(5837), 502–507, doi:10.1126/science.1139994.

Marzin, C., N. Kallel, M. Kageyama, J.-C. Duplessy, and P. Braconnot (2013), Glacial fluctuations of the Indian monsoon and their relationship with North Atlantic climate: new data and modelling experiments, Clim. Past, 9(5), 2135–2151, doi:10.5194/cp-9-2135-2013.

Moreno, E., N. Thouveny, D. Delanghe, I. N. McCave, and N. J. Shackleton (2002), Climatic and oceanographic changes in the Northeast Atlantic reflected by magnetic properties of sediments deposited on the Portuguese Margin during the last 340 ka, Earth Planet. Sci. Lett., 202(2), 465–480, doi:10.1016/S0012-821X(02)00787-2.

NEEM Community Members (2013), Eemian interglacial reconstructed from a Greenland folded ice core, Nature, 493(7433), 489–494, doi:10.1038/nature11789.

Otto-Bliesner, B. L. et al. (2009), A comparison of PMIP2 model simulations and the MARGO proxy reconstruction for tropical sea surface temperatures at last glacial maximum, Clim. Dyn., 32(6), 799–815, doi:10.1007/s00382-008-0509-0.

Paillard, D., L. Labeyrie, and P. Yiou (1996), Macintosh program performs time-series analysis, Eos Transanctions AGU, 77(379).

Pailler, D., and E. Bard (2002), High frequency palaeoceanographic changes during the past 140000 yr recorded by the organic matter in sediments of the Iberian Margin, Palaeogeogr. Palaeoclimatol. Palaeoecol., 181(4), 431–452, doi:10.1016/S0031-0182(01)00444-8.

Pires, A. C., R. Nolasco, A. Rocha, A. M. Ramos, and J. Dubert (2014), Global climate models as forcing for regional ocean modeling: a sensitivity study in the Iberian Basin (Eastern North Atlantic), Clim. Dyn., 43(3-4), 1083–1102, doi:10.1007/s00382-014-2151-3.

Prahl, F. G., and S. G. Wakeham (1987), Calibration of unsaturation patterns in long-chain ketone compositions for palaeotemperature assessment, Nature, 330(6146), 367–369, doi:10.1038/330367a0.

Rasmussen, S. O. et al. (2006), A new Greenland ice core chronology for the last glacial termination, J. Geophys. Res. Atmospheres, 111(D6), D06102, doi:10.1029/2005JD006079.

Rasmussen, S. O. et al. (2014), A stratigraphic framework for abrupt climatic changes during the Last Glacial period based on three synchronized Greenland ice-core records: refining and extending the INTIMATE event stratigraphy, Quat. Sci. Rev., 106, 14–28, doi:10.1016/j.quascirev.2014.09.007.

Rosell-Melé, A. et al. (2001), Precision of the current methods to measure the alkenone proxy U37K′ and absolute alkenone abundance in sediments: Results of an interlaboratory comparison study, *Geochem. Geophys. Geosystems*, *2*(7), 1046, doi:10.1029/2000GC000141.

Salgueiro, E., A. Voelker, L. de Abreu, F. Abrantes, H. Meggers, and G. Wefer (2010), Temperature and productivity changes off the western Iberian margin during the last 150 ky, *Quat. Sci. Rev.*, *29*(5-6), 680–695, doi:10.1016/j.quascirev.2009.11.013.

Sánchez Goñi, M. F. (2006), Interactions végétation-climat au cours des derniers 425.000 ans en Europe occidentale. Le message du pollen des archives marines, *Quat. Rev. Assoc. Fr. Pour Létude Quat.*, (vol. 17/1), 3–25, doi:10.4000/quaternaire.585.

Sánchez Goñi, M. F., F. Eynaud, J. L. Turon, and N. J. Shackleton (1999), High resolution palynological record off the Iberian margin: direct land-sea correlation for the Last Interglacial complex, *Earth Planet. Sci. Lett.*, *171*(1), 123–137, doi:10.1016/S0012-821X(99)00141-7.

Sánchez Goñi, M. F., J.-L. Turon, F. Eynaud, and S. Gendreau (2000), European Climatic Response to Millennial-Scale Changes in the Atmosphere–Ocean System during the Last Glacial Period, *Quat. Res.*, *54*(3), 394–403, doi:10.1006/qres.2000.2176.

Sánchez Goñi, M. F., I. Cacho, J. Turon, J. Guiot, F. Sierro, J. Peypouquet, J. Grimalt, and N. Shackleton (2002), Synchroneity between marine and terrestrial responses to millennial scale climatic variability during the last glacial period in the Mediterranean region, *Clim. Dyn.*, *19*(1), 95–105, doi:10.1007/s00382-001-0212-x.

Sánchez Goñi, M. F., M. F. Loutre, M. Crucifix, O. Peyron, L. Santos, J. Duprat, B. Malaizé, J.-L. Turon, and J.-P. Peypouquet (2005), Increasing vegetation and climate gradient in Western Europe over the Last Glacial Inception (122–110 ka): data-model comparison, *Earth Planet. Sci. Lett.*, *231*(1–2), 111–130, doi:10.1016/j.epsl.2004.12.010.

Sánchez Goñi, M. F., A. Landais, W. J. Fletcher, F. Naughton, S. Desprat, and J. Duprat (2008), Contrasting impacts of Dansgaard-Oeschger events over a western European latitudinal transect modulated by orbital parameters, *Quat. Sci. Rev.*, *27*(11-12), 1136–1151, doi:10.1016/j.quascirev.2008.03.003.

Sánchez Goñi, M. F., A. Landais, I. Cacho, J. Duprat, and L. Rossignol (2009), Contrasting intrainterstadial climatic evolution between high and middle North Atlantic latitudes: A close-up of Greenland Interstadials 8 and 12, *Geochem. Geophys. Geosystems*, *10*, Q04U04, doi:10.1029/2008GC002369.

Sánchez Goñi, M. F., E. Bard, A. Landais, L. Rossignol, and F. d'Errico (2013), Air-sea temperature decoupling in western Europe during the last interglacial-glacial transition, *Nat. Geosci.*, *6*(10), 837–841, doi:10.1038/ngeo1924.

Savitzky, A., and M. J. E. Golay (1964), Smoothing and Differentiation of Data by Simplified Least Squares Procedures., *Anal. Chem.*, *36*(8), 1627–1639, doi:10.1021/ac60214a047.

Seierstad, I. K. et al. (2014), Consistently dated records from the Greenland GRIP, GISP2 and NGRIP ice cores for the past 104 ka reveal regional millennial-scale δ18O gradients with possible Heinrich event imprint, Quat. Sci. Rev., 106, 29–46, doi:10.1016/j.quascirev.2014.10.032.

Shackleton, N. J., M. A. Hall, and E. Vincent (2000), Phase relationships between millennial-scale events 64,000-24,000 years ago, Paleoceanography, 15(6), 565–569, doi:10.1029/2000PA000513.

Shackleton, N. J., M. Chapman, M. F. Sánchez-Goñi, D. Pailler, and Y. Lancelot (2002), The Classic Marine Isotope Substage 5e, Quat. Res., 58(1), 14–16, doi:10.1006/qres.2001.2312.

Shackleton, N. J., M. F. Sánchez-Goñi, D. Pailler, and Y. Lancelot (2003), Marine Isotope Substage 5e and the Eemian Interglacial, Glob. Planet. Change, 36(3), 151–155, doi:10.1016/S0921-8181(02)00181-9.

Shackleton, N. J., R. G. Fairbanks, T. Chiu, and F. Parrenin (2004), Absolute calibration of the Greenland time scale: implications for Antarctic time scales and for Δ14C, Quat. Sci. Rev., 23(14–15), 1513–1522, doi:10.1016/j.quascirev.2004.03.006.

Skinner, L. C., and I. N. McCave (2003), Analysis and modelling of gravity- and piston coring based on soil mechanics, Mar. Geol., 199(1-2), 181–204, doi:10.1016/S0025-3227(03)00127-0.

Sonzogni, C., E. Bard, F. Rostek, R. Lafont, A. Rosell-Mele, and G. Eglinton (1997), Core-top calibration of the alkenone index vs sea surface temperature in the Indian Ocean, Deep Sea Res. Part II Top. Stud. Oceanogr., 44(6–7), 1445–1460, doi:10.1016/S0967-0645(97)00010-6.

Steffensen, J. P. et al. (2008), High-resolution Greenland Ice Core data show abrupt climate change happens in few years, Science, 321(5889), 680–684, doi:10.1126/science.1157707.

Svensson, A. et al. (2006), The Greenland Ice Core Chronology 2005, 15–42 ka. Part 2: comparison to other records, Quat. Sci. Rev., 25(23–24), 3258–3267, doi:10.1016/j.quascirev.2006.08.003.

Svensson, A. et al. (2008), A 60 000 year Greenland stratigraphic ice core chronology, Clim. Past, 4(1), 47–57, doi:10.5194/cp-4-47-2008.

Thouveny, N., E. Moreno, D. Delanghe, L. Candon, Y. Lancelot, and N. J. Shackleton (2000), Rock magnetic detection of distal ice-rafted debries: clue for the identification of Heinrich layers on the Portuguese margin, Earth Planet. Sci. Lett., 180(1-2), 61–75, doi:10.1016/S0012-821X(00)00155-2.

Thouveny, N., J. Carcaillet, E. Moreno, G. Leduc, and D. Nerini (2004), Geomagnetic moment variation and paleomagnetic excursions since 400 kyr BP: a stacked record from sedimentary sequences of the Portuguese margin, Earth Planet. Sci. Lett., 219(3-4), 377–396, doi:10.1016/S0012-821X(03)00701-5.

Vinther, B. M. et al. (2006), A synchronized dating of three Greenland ice cores throughout the Holocene, J. Geophys. Res. Atmospheres, 111(D13), D13102, doi:10.1029/2005JD006921.

Voelker, A. H. L., and L. de Abreu (2011), A Review of Abrupt Climate Change Events in the Northeastern Atlantic Ocean (Iberian Margin): Latitudinal, Longitudinal, and Vertical

Gradients, in *Abrupt Climate Change: Mechanisms, Patterns , and Impacts*, vol. 193, edited by H. Rashid, L. Polyak, and E. Mosley-Thompson, pp. 15–37, American Geophysical Union, Washington, D. C.

Wang, Y., H. Cheng, R. L. Edwards, X. Kong, X. Shao, S. Chen, J. Wu, X. Jiang, X. Wang, and Z. An (2008), Millennial- and orbital-scale changes in the East Asian monsoon over the past 224,000 years, *Nature*, *451*(7182), 1090–1093, doi:10.1038/nature06692.

Wang, Y. J., H. Cheng, R. L. Edwards, Z. S. An, J. Y. Wu, C.-C. Shen, and J. A. Dorale (2001), A High-Resolution Absolute-Dated Late Pleistocene Monsoon Record from Hulu Cave, China, *Science*, *294*(5550), 2345 –2348, doi:10.1126/science.1064618.

Woillez, M.-N., M. Kageyama, N. Combourieu-Nebout, and G. Krinner (2013), Simulating the vegetation response in western Europe to abrupt climate changes under glacial background conditions, *Biogeosciences*, *10*(3), 1561–1582, doi:10.5194/bg-10-1561-2013.

Zhang, R., and T. L. Delworth (2005), Simulated tropical response to a substantial weakening of the Atlantic thermohaline circulation, *J. Clim.*, *18*(12), 1853–1860, doi:10.1175/JCLI3460.1.